



DOI 10.24425/ae.2022.140195

## Model predictive direct power control of energy storage quasi-Z-source grid-connected inverter

MIN'AN TANG<sup>1</sup>, SHANGMEI YANG<sup>2</sup>  , KAIYUE ZHANG<sup>1</sup>, QIANQIAN WANG<sup>3</sup>,  
CHENGGANG LIU<sup>4</sup>, XUEWANG DONG<sup>5</sup>

<sup>1</sup>*School of Automation and Electrical Engineering, Lanzhou Jiaotong University  
China*

<sup>2</sup>*College of Electrical Engineering, Lanzhou Institute of Technology  
China*

<sup>3</sup>*College of Electrical and Information Engineering, Lanzhou University of Technology  
China*

<sup>4</sup>*Gansu Province Special Equipment Inspection and Testing Institute  
China*

<sup>5</sup>*Jingtaichuan Electric Power Pumping Irrigation Water Resources Utilization Center of Gansu Province  
China*

*e-mail: 2669686284@qq.com*

(Received: 20.05.2021, revised: 23.08.2021)

**Abstract:** In order to overcome the shortcoming of large switching losses caused by variable switching frequency appears in the conventional finite control set model predictive control (FCS-MPC) algorithm, a model predictive direct power control (MP-DPC) for an energy storage quasi-Z-source inverter (ES-qZSI) is proposed. Firstly, the power prediction model of the ES-qZSI is established based on the instantaneous power theory. Then the average voltage vector in the  $\alpha\beta$  coordinate system is optimized by the power cost function. Finally, the average voltage vector is used as the modulation signal, and the corresponding switching signal with fixed frequency is generated by the shoot-through segment space vector pulse width modulation (SVPWM) technology. The simulation results show that the ES-qZSI realizes six shoot-through actions per control cycle and achieves the constant frequency control of the system, which verifies the correctness of the proposed control strategy.

**Key words:** energy-stored quasi-Z-source inverter, constant frequency control, model predictive direct power control, space vector modulation module



© 2022. The Author(s). This is an open-access article distributed under the terms of the Creative Commons Attribution-NonCommercial-NoDerivatives License (CC BY-NC-ND 4.0, <https://creativecommons.org/licenses/by-nc-nd/4.0/>), which permits use, distribution, and reproduction in any medium, provided that the Article is properly cited, the use is non-commercial, and no modifications or adaptations are made.

## 1. Introduction

With the increasing contradiction of environmental pollution and energy structure imbalance, the renewable energy power generation technology represented by solar energy has been widely studied by scholars at home and abroad [1]. As the core component of renewable energy and power grid, inverter's topology and control strategy directly affect power transmission quality of the grid-connected system. A quasi-Z-source inverter (qZSI) not only inherits a single-stage boosted and contravariant function of the Z-source inverter, but also has the unique advantages of continuous input current and a low device voltage level, so it is widely used in the photovoltaic power generation system [2–4]. However, photovoltaic output power is affected by the fluctuations of external environment, which will lead to unbalanced grid-connected voltage and increased current harmonics [5,6]. Therefore, it is necessary to add energy storage devices in the system to improve above problems. In reference [7], a qZSI topology that paralleled the energy storage device to the capacitor  $C_1$  is proposed to realize energy storage without an additional converter and charge-discharge circuit. Through the introduction of an energy storage device to realize bidirectional flow of system power, the power balance of the energy storage quasi-Z-source inverter (ES-qZSI) system is adjusted, the impact of photovoltaic power fluctuation on the grid is reduced, and investment cost is reduced [8,9]. Based on the advantages of the ES-qZSI structure compared with the traditional grid-connected inverter, this paper chooses the inverter to connect PV array and power grid to achieve a high-performance grid-connected inverter system.

Direct power control (DPC) is widely studied by scholars because of its easy implementation, a low-current distortion rate and fast dynamic response [10–12]. However, the traditional DPC system generally uses a power hysteresis comparator and switching vector table to select a voltage vector. This method of controlling a switch tube will increase switching losses of the system and generate additional harmonics, which makes the filter design difficult [13]. Therefore, relevant scholars propose to introduce model predictive control into DPC algorithm, so that the space vector pulse width modulation (SVPWM) technology can be effectively combined with DPC. While the switching frequency of a DPC is fixed, it also maintains its fast-dynamic power tracking response characteristics. Therefore, it is applied in many fields such as the PWM rectifier, three-phase grid-connected inverter, single-phase three-level pulse rectifier, AC/DC converter and other fields [14–18]. In view of the problem that the switching frequency of MP-DPC is not fixed, the constant frequency model predictive power control of three-phase PWM rectifier is realized by combining space vector pulse width modulation in reference [19], which effectively reduces switching losses and current harmonics of the system. In reference [20], a finite switching sequence model predictive direct power control method is proposed to realize the fixed frequency control of an energy storage quasi-Z-source inverter.

Based on the above analysis, a model predictive direct power control (MP-DPC) strategy for an energy storage quasi-Z-source a photovoltaic grid-connected inverter is studied. In this method, instantaneous value of active and reactive power output by the inverter is used as controlled variable, and the average voltage vector in the  $\alpha\beta$  coordinate system is obtained by the model predictive controller. The average voltage vector is sent into the shoot-through segment SVPWM module to modulate fixed switching signal. Finally, photovoltaic grid-connected system model of an energy storage quasi-Z-source inverter is built, and the effectiveness of the proposed control strategy is verified by simulation.

## 2. Power prediction model of ES-qZSI

The photovoltaic grid-connected topology of an energy storage quasi-Z-source inverter is shown in Fig. 1. The system consists of PV array, energy storage battery and quasi-Z-source three-phase inverter bridge. The inverter is connected to the AC side grid through filter inductor.  $e_a, e_b, e_c$  represent three-phase grid-side voltage.

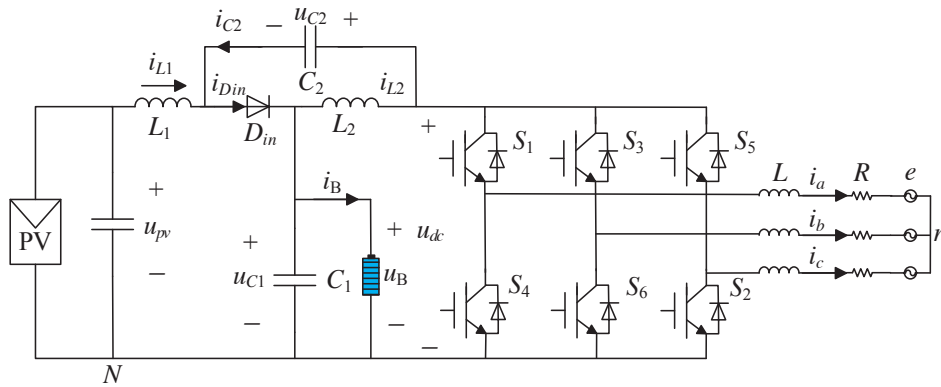


Fig. 1. Topology of Energy-stored quasi-Z-source photovoltaic grid-connected inverter

The ES-qZSI has two working states of non-shoot-through and shoot-through [21], and its equivalent circuit is shown in Fig. 2(a) and Fig. 2(b). When the ES-qZSI works in the shoot-through state, the diode is turned off because its applied voltage is the reverse voltage. At this time, the photovoltaic cell and capacitor provide electric energy to the inductor at the same time, and the inverter and power grid can be equivalent to one conductor. When the ES-qZSI works in the non-shoot-through state, the diode is turned on because its applied voltage is a positive voltage. At this time, both PV cell and inductor provide electric energy to the capacitor, and additional energy is supplied to the load. The inverter and power grid can be equivalent to a constant current source, and the inverter bridge works in one of the eight traditional effective switching states.

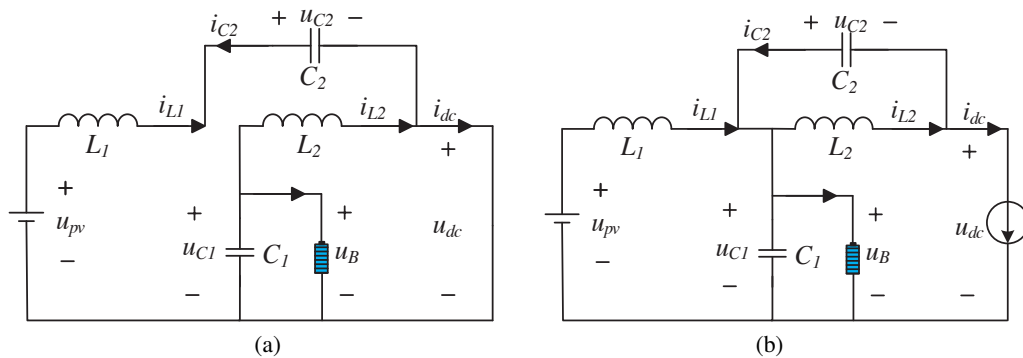


Fig. 2. DC equivalent circuit of ES-qZSI: shoot-through state (a); non-shoot-through state (b)

Assuming that the diodes, inductors and capacitors in the impedance source network are ideal components, the state equation of the impedance source network in the shoot-through state can be deduced according to Kirchhoff's voltage law, as shown in Eq. (1):

$$u_{L1} = u_{pv} + u_{C2}, \quad u_{L1} = u_{C1}, \quad u_{dc} = 0. \quad (1)$$

Similarly, the state equation of impedance source network in the non-shoot-through state as shown in Eq. (2):

$$u_{L1} = u_{pv} - u_{C1}, \quad u_{L2} = -u_{C2}, \quad u_{dc} = u_{C1} + u_{C2}. \quad (2)$$

$D = \frac{T_{sh}}{T_s}$  is defined as a shoot-through duty cycle, which represents the acting time of the shoot-through state in one control cycle. The relationship between  $u_{dc}$ ,  $u_{C1}$ ,  $u_{C2}$  and  $u_{pv}$  of the ES-qZSI system at a steady state can be obtained from the average voltage of inductance equal to 0 in one cycle (volt second balance principle) as shown in Eq. (3):

$$\begin{cases} u_{C1} = \frac{1-D}{1-2D}u_{pv} \\ u_{C2} = \frac{D}{1-2D}u_{pv} \\ u_{dc} = u_{C1} + u_{C2} = \frac{1}{1-2D}u_{pv} = Bu_{pv} \end{cases}, \quad (3)$$

where  $u_{dc}$  is the DC link voltage of the ES-qZSI in the non-shoot-through state. From Formula (3), it can be seen that due to the addition of shoot-through state,  $u_{dc}$  is  $B$  times of the input  $u_{pv}$ , and  $B$  is defined as the boost coefficient. Therefore, the peak output AC voltage of the energy storage quasi-Z-source inverter as shown in Eq. (4):

$$u_m = \frac{1}{2}u_{dc}M = \frac{1}{2}MBu_{pv}, \quad (4)$$

where  $M$  represents the modulation ratio.

Since there is a certain coupling relationship between  $M$  and  $D$ , this paper adopts a shoot through segment SVPWM to improve utilization rate of DC voltage and reduce switching frequency of the system.

The output current prediction model of three-phase inverter in the  $\alpha\beta$  coordinate can be expressed as Eq. (5):

$$\begin{cases} \frac{di_\alpha}{dt} = \frac{1}{L}(u_{\alpha n} - Ri_\alpha - e_\alpha) \\ \frac{di_\beta}{dt} = \frac{1}{L}(u_{\beta n} - Ri_\beta - e_\beta) \end{cases}, \quad (5)$$

where  $e_\alpha$  and  $e_\beta$  are the  $\alpha$  and  $\beta$  components of grid-side voltage.

Assuming three-phase network voltage is balanced, the calculation formula of the output  $P$  and  $Q$  of the ES-qZSI at  $k$  time can be calculated according to the instantaneous power theory, as shown in Formula (6):

$$\begin{cases} P(t) = \frac{3}{2}(e_\alpha i_\alpha + e_\beta i_\beta) \\ [6pt] Q(t) = \frac{3}{2}(e_\beta i_\alpha - e_\alpha i_\beta) \end{cases}. \quad (6)$$

The power change rate can be calculated by Eq. (7):

$$\begin{cases} \frac{dP(t)}{dt} = \frac{3}{2} \left( i_\alpha \frac{de_\alpha}{dt} + e_\alpha \frac{di_\alpha}{dt} + i_\beta \frac{de_\beta}{dt} + e_\beta \frac{di_\beta}{dt} \right) \\ \frac{dQ(t)}{dt} = \frac{3}{2} \left( i_\alpha \frac{de_\beta}{dt} + e_\beta \frac{di_\alpha}{dt} - i_\beta \frac{de_\alpha}{dt} - e_\alpha \frac{di_\beta}{dt} \right) \end{cases} \quad (7)$$

Under the condition of three-phase voltage balance and pure sinusoidal waveform, an instantaneous change rate of voltage is defined as Eq. (8):

$$\begin{cases} \frac{de_\alpha}{dt} = -\omega e_\beta \\ \frac{de_\beta}{dt} = \omega e_\alpha \end{cases} \quad (8)$$

Bring Formulas (7) and (8) into Formula (6), then the expressions of  $P$  and  $Q$  can be deduced as Formula (9):

$$\begin{cases} \frac{dP(t)}{dt} = \frac{3}{2L} \left( e_\alpha^2 - e_\alpha u_\alpha - \operatorname{Re}_\alpha i_\alpha + e_\beta^2 - e_\beta u_\beta - \operatorname{Re}_\beta i_\beta \right) + \omega (e_\alpha i_\beta - e_\beta i_\alpha) \\ \frac{dQ(t)}{dt} = \frac{3}{2L} \left( e_\alpha u_\beta - e_\beta u_\alpha + \operatorname{Re}_\alpha i_\beta - \operatorname{Re}_\beta i_\alpha \right) + \omega (e_\alpha i_\alpha + e_\beta i_\beta) \end{cases} \quad (9)$$

Suppose that the values of  $P$  and  $Q$  derivatives at  $k$  time are  $X$  and  $Y$ , then Formula (9) is defined as Formula (10):

$$\begin{cases} \left. \frac{dP(t)}{dt} \right|_{t=k} = \frac{P(k+1) - P(k)}{T_s} = X \\ \left. \frac{dQ(t)}{dt} \right|_{t=k} = \frac{Q(k+1) - Q(k)}{T_s} = Y \end{cases} \quad (10)$$

The predicted values of active and reactive power at  $k+1$  time are shown in Eq. (11):

$$\begin{cases} P(k+1) = XT_s + P(k) \\ Q(k+1) = YT_s + Q(k) \end{cases} \quad (11)$$

### 3. MP-DPC strategy

MP-DPC is divided into two parts: voltage outer loop control and power inner loop control. It is mainly composed of a system sampling circuit, instantaneous power control, model predictive controller, shoot-through segment SVPWM module and PI regulator. An ES-qZSI system control block diagram is shown in Fig. 3.

The working principle of control strategy is as follows: input voltage  $u_{pv}$  and current  $i_{L1}$  are sampled, input voltage is stabilized by a photovoltaic power control module, and shoot-through duty cycle  $D$  is obtained. Grid voltage and current are sampled and converted into voltage  $e_\alpha$ ,  $e_\beta$  and current  $i_\alpha$ ,  $i_\beta$  in  $\alpha\beta$  coordinate by coordinate transformation. Instantaneous values of  $P$

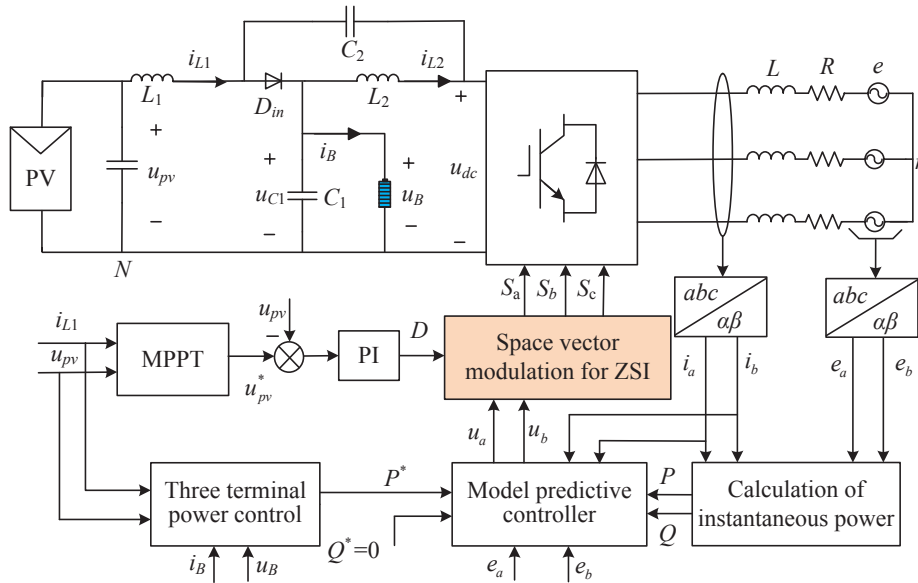


Fig. 3. MP-DPC structure block diagram of ES-qZSI

and  $Q$  are obtained by the instantaneous power calculation formula, and then power reference value  $P^*$  is obtained from a three-terminal power calculation module. In order to realize a unit power grid connection, let  $Q^* = 0$ . Taking  $e_\alpha, e_\beta, i_\alpha, i_\beta, P^*$  and  $Q^* = 0$  as the input of a model predictive controller, the tracking error between instantaneous power and given power reference value is eliminated by a model predictive algorithm, and then average voltage vectors  $u_\alpha$  and  $u_\beta$  required for each switching cycle are obtained. The voltage vector and the duty cycle  $D$  obtained by photovoltaic power control are modulated by space vector modulation for qZSI to obtain a corresponding switching state, and the switching state is applied to the inverter control in the next cycle to achieve the goal of grid-connected current tracking without static error and fixed switching frequency control.

### 3.1. Three terminal power control

The ES-qZSI system belongs to a three-terminal power balance mode (photovoltaic power, battery power and grid-connected power control). The photovoltaic power control module uses MPPT control to obtain maximum power point voltage, and the voltage is used as input voltage reference value of system. The difference between the reference value and actual value of the input voltage is adjusted by a PI controller. Shoot-through duty cycle  $D$  is shown in Eq. (12):

$$D = k_p (u_{pv}^* - u_{pv}) + k_i \int (u_{pv}^* - u_{pv}) dt, \quad (12)$$

where  $k_p$  and  $k_i$  are the proportional and integral coefficients of the output voltage controller of the photovoltaic array. The shoot-through duty cycle can realize maximum power tracking and boost control of the inverter through space vector modulation for the qZSI.

The battery power control module realizes the purpose of flexibly adjusting the power difference between the system input power and the grid connected power and stabilizing the power fluctuation of photovoltaic and power grid through reasonable energy management of the energy storage quasi-Z-source inverter [22]. The reference value of output current can be obtained from the power balance equation, as shown in Formula (13):

$$P^* = u_{pv}i_{L1} - u_B i_B^*, \quad (13)$$

where  $u_B$  and  $i_B$  are the battery voltage and current.

During energy management of energy storage quasi-Z-source inverter, it is necessary to ensure that the state of charge (SOC) of the battery works within a reasonable range without charge and discharge. The SOC value is the ratio of the remaining capacity of the battery to its rated capacity. The battery can operate in three working states: charging state, no charge and discharge state and discharge state [23]. The power flow direction of the system is shown in Fig. 4.

1. State of charge: the grid power is less than the power output by the PV array, and the remaining power is absorbed by the battery, that is,  $i_B > 0$ ,  $i_{L1} > i_{L2}$ ,  $P_B > 0$ ,  $P_{pv} > P_{out}$ .
2. No charge and discharge state: the output power of PV array is equal to the power grid, and the battery is neither charged nor discharged, that is,  $i_B = 0$ ,  $i_{L1} = i_{L2}$ ,  $P_B = 0$ ,  $P_{pv} = P_{out}$ .
3. Discharge state: the grid power is greater than the power output by the PV array, and the missing power will be supplemented by the battery, that is,  $i_B < 0$ ,  $i_{L1} < i_{L2}$ ,  $P_B < 0$ ,  $P_{pv} < P_{out}$ .

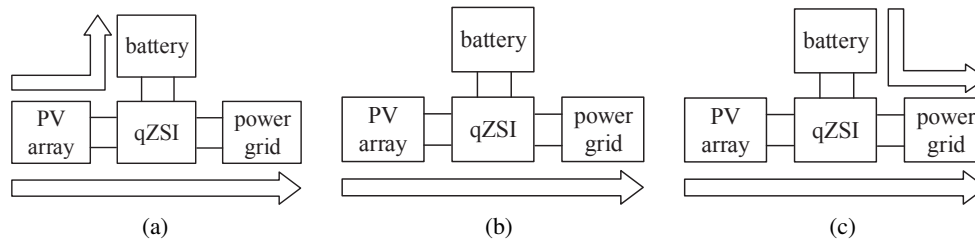


Fig. 4. System power flow direction: state of charge (a); no charge and discharge state (b); discharge state (c)

The selection basis for parameters of the battery: due to

$$u_B = u_{C1} = \frac{1-D}{1-2D} u_{pv},$$

when  $u_{dc} = 800$  V and  $u_{pv} = 533.28$  V, they can be obtained according to Eq (3). At this time, the through duty cycle of the ES-qZSI system  $D = 0.197$  and  $u_B = 707$  V. Therefore, the rated capacity and rated voltage of the battery are set to 40 Ah and 707 V, respectively, and the initial SOC percentage is 80%.

### 3.2. Model predictive controller

The average voltage vector of the inverter can be obtained by introducing a model predictive control algorithm. The voltage vector is modulated by space vector modulation for a qZSI, which can modulate signal of switching control switch, so as to realize constant frequency control of

the ES-qZSI system. Therefore, it is necessary to design a cost function and minimize it to obtain optimal values of average voltage vectors  $u_\alpha$  and  $u_\beta$ . The cost function is shown in Eq. (14):

$$g = [P^*(k) - P(k+1)]^2 + [Q^*(k) - Q(k+1)]^2. \quad (14)$$

In order to reduce power tracking error, the optimal voltage vector corresponding to minimizing the cost function  $g$  is obtained by setting

$$\frac{\partial g}{\partial u_\alpha} = 0, \quad \frac{\partial g}{\partial u_\beta} = 0.$$

The partial derivatives of the cost function to  $u_\alpha$  and  $u_\beta$  are shown in Formula (15):

$$\begin{cases} \frac{\partial g}{\partial u_\alpha} = T_s \left[ \frac{3e_\alpha}{L} (P^*(k) - P(k) - XT_s) \right] + T_s \left[ \frac{3e_\beta}{L} (Q^*(k) - Q(k) - YT_s) \right] \\ \frac{\partial g}{\partial u_\beta} = T_s \left[ \frac{3e_\beta}{L} (P^*(k) - P(k) - XT_s) \right] - T_s \left[ \frac{3e_\alpha}{L} (Q^*(k) - Q(k) - YT_s) \right] \end{cases}. \quad (15)$$

Let Eq. (15) be equal to 0, then output voltage vectors  $u_\alpha$  and  $u_\beta$  of the inverter are shown in Formula (16):

$$\begin{cases} u_\alpha(k) = \frac{e_\alpha^3 + e_\alpha e_\beta^2}{e_\alpha^2 + e_\beta^2} - Ri_\alpha + \frac{2}{3}L\omega i_\beta - \frac{2L}{3T_s(e_\alpha^2 + e_\beta^2)} [e_\alpha e_P(k) + e_\beta e_Q(k)] \\ u_\beta(k) = \frac{e_\beta^3 + e_\beta e_\alpha^2}{e_\alpha^2 + e_\beta^2} - Ri_\beta - \frac{2}{3}L\omega i_\alpha - \frac{2L}{3T_s(e_\alpha^2 + e_\beta^2)} [e_\beta e_P(k) - e_\alpha e_Q(k)] \end{cases}, \quad (16)$$

where  $e_P(k) = P^*(k) - P(k)$  and  $e_Q(k) = Q^*(k) - Q(k)$ .

After calculating the average voltage vector of the inverter in each control cycle, the corresponding switching state is obtained by the space vector modulation for the qZSI.

### 3.3. Space vector modulation for qZSI

The traditional SVPWM strategy belongs to buck modulation, and the maximum amplitude of its reference voltage is limited to the effective voltage vector (the maximum value can be taken as  $\frac{u_{dc}}{\sqrt{3}}$ ). Therefore, the traditional SVM is not suitable for the ES-qZSI that needs to achieve voltage buck-boost function. According to the different number of distribution segments in the shoot through state, the existing research on the space vector modulation for a qZSI can be divided into three types: ZSVM2, ZSVM4 and ZSVM6. The three ZSVM methods are compared and analyzed in the reference [24] on the switching modulation mode, the maximum voltage stress and the maximum shoot through duty cycle. It is concluded that ZSVM6 can fully utilize zero vector action time, and because it inserts multi-segment shoot-through times in in per control cycle, the inductor current ripple is small and the modulation factor range is wide, so it has better comprehensive performance. Therefore, ZSVM6 strategy is mainly used in the space vector modulation for a qZSI to achieve fixed switching frequency and reduce switching losses.



The ZSVM6 strategy of a three-phase energy storage quasi-Z-source inverter, under the premise of ensuring the active time  $T_1$  and  $T_2$  of the active voltage vectors  $\mathbf{u}_1$  and  $\mathbf{u}_2$  unchanged, reasonably inserts six equal parts of shoot-through time  $T_{sh}$  into the conversion time of the traditional zero vector and active vector, making full use of the operation time of the traditional zero vector. If only a single-phase bridge arm is shoot-through in each switching cycle, three shoot-through zero vectors,  $\mathbf{u}_{s1}$ ,  $\mathbf{u}_{s2}$  and  $\mathbf{u}_{s3}$  are generated, without increasing its switching frequency and switching losses [25, 26]. The space voltage vector of an ES-qZSI is shown in Fig. 5(a). It can be seen that the modulation range of the reference voltage vector can be extended to the outer circle (that is, the value range of  $|\mathbf{U}_M^*|$  can be increased to  $B \frac{u_{dc}}{\sqrt{3}}$ ) due to the insertion of shoot-through zero vector  $\mathbf{u}_{sh}$ , which effectively uses the dc-link voltage, and achieves the purpose of boost control on the premise of realizing the through mode. The switch sequence of the ZSVM6 strategy is shown in Fig. 5(b).

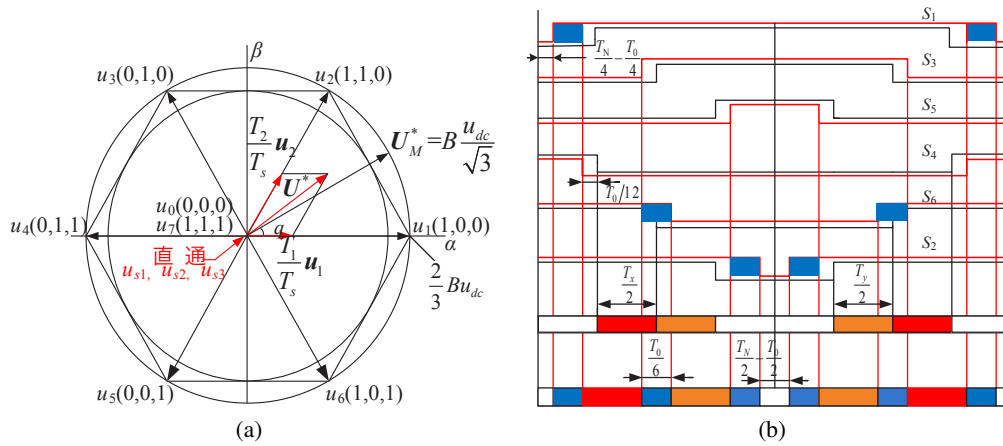


Fig. 5. ZSVM6 strategy of the ES-qZSI in sector I: synthesis schematic diagram of ZSVM6 (a); switch sequence of ZSVM6 (b)

After considering the shoot-through state, the expression of the reference voltage vector of the first sector can be obtained, as shown in Eq. (17):

$$\mathbf{u}^* = \mathbf{u}_1 \frac{T_1}{T_s} + \mathbf{u}_2 \frac{T_2}{T_s} + \mathbf{u}_0 \frac{T_0}{T_s} + \mathbf{u}_{sh} \frac{T_{sh}}{T_s}. \tag{17}$$

Since  $\mathbf{u}_0$  and  $\mathbf{u}_{sh}$  are not involved in the synthesis of  $\mathbf{u}^*$ , actuation duration of each vector is derived as Eq. (18):

$$T_s = T_1 + T_2 + \bar{T}_0 + T_{sh}, \quad \mathbf{u}_0 \frac{T_0}{T_s} + \mathbf{u}_{sh} \frac{T_{sh}}{T_s} = 0. \tag{18}$$

It can be seen from Eq. (17) and Eq. (18) that the reference voltage vector of the ES-qZSI before and after inserting the shoot-through vector remains unchanged.

The blue region in the Fig. 5(b) represents the action time of six inserted through vectors, and red and yellow regions represent the action time of two active voltage vectors, which are the

same as the time interval  $T_x/2$  and  $T_y/2$  of the traditional SVPWM. The white region represents the action time of the zero vector, and the time interval is  $T_0/4$ . The specific control process is as follows: in the first half cycle of sector I, switch  $S_1$  is turned on for  $T_{sh}/4$  in advance to generate the first-stage through, and  $S_6$  is delayed to turn off  $T_{sh}/12$  to generate the second-stage through. However, this state takes up the action time of the effective vector  $\{110\}$   $T_{sh}/12$ . In order not to change the action time of this vector,  $S_2$  needs to be delayed by  $T_{sh}/12$  before turning off, and at the same time delaying  $T_{sh}/12$  for turning off to generate the third stage through, the switching principle of the second half cycle and the remaining five sectors is the same as the above.

## 4. Simulation results

According to the principle of the MP-DPC strategy, the simulation model of the MP-DPC strategy system of an energy storage quasi-Z-source inverter is built in MATLAB/Simulink to verify the feasibility and effectiveness of the proposed method. The main parameters of the ES-qZSI system are shown in Table 1.

Table 1. Simulation parameters of system

Parameter name	Symbol	Value	Unit
Grid voltage	$e$	380	V
Input voltage	$u_{pv}$	540	V
Capacity of energy storage battery	$C$	40	AH
Battery voltage	$u_B$	707	V
Internal resistance of photovoltaic cells	$r_s$	2.58	$\Omega$
Quasi-Z-source source network inductance	$L_1, L_2$	1	mH
Quasi-Z-source source network capacitance	$C_1, C_2$	3000, 800	$\mu\text{F}$
Sampling frequency	$f$	10	kHz

### 4.1. Simulation results of DC side

The ES-qZSI is set to operate under the condition that the ambient temperature remains unchanged at 25°C, the light intensity increases from 800 W/m<sup>2</sup> to 1 kW/m<sup>2</sup> at 0.5 s, and decreases from 1 kW/m<sup>2</sup> to 600 W/m<sup>2</sup> at 1 s. The simulation results of its DC side are shown in Fig. 6.

Figure 6(a) shows the inductance current waveform when the light intensity changes. It can be seen that the inductance current increases from 84 A to 106 A at 0.5 s, and decreases from 106 A to 64 A at 1 s. Figure 6(b) shows the current waveform of the battery under the change of photovoltaic power. The battery current changes from -14 A (discharged state) to 2 A (charged state) at 0.5 s, and from 2 A (charged state) to -30 A (discharged state) in 1 s. It can be seen from Fig. 6(c) that when the PV conditions change, the PV cell always runs at the maximum power point due to MPPT control, and the photovoltaic voltage is 538 V. Figure 6(d) shows

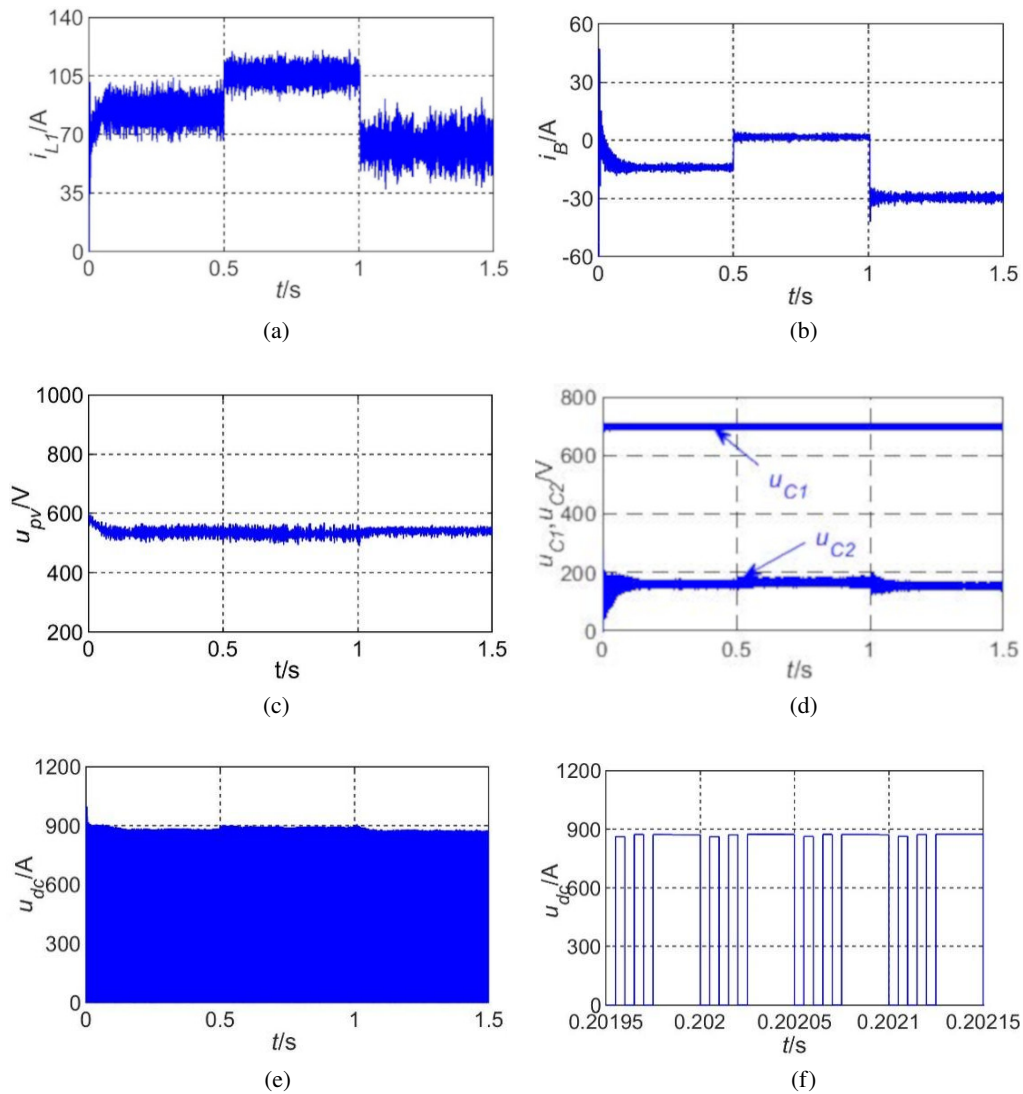


Fig. 6. Simulation results for DC side of ES-qZSI: current waveform of inductance  $L_1$  (a); current waveform of battery (b); voltage waveform of PV (c); voltage waveform of inductance  $C_1$  and  $C_2$  (d); voltage waveform of DC link (e); partial enlarged waveform of DC link voltage (f)

that the voltage of capacitor  $C_1$  and  $C_2$  in the ES-qZSI network is constant, and the voltage of capacitor  $C_1$  is approximately equal to the terminal voltage of the energy storage battery, which is 707 V. Figure 6(e) is the waveform of the DC side voltage  $u_{dc}$ . It can be seen that  $u_{dc}$  changes periodically between the maximum value of 900 V and 0 V, and its maximum value is the sum of two capacitance voltages, which realizes the maximum boost of the ES-qZSI without increasing the switching frequency. In each control cycle, the ES-qZSI realizes six shoot-through actions.

As shown in the partial enlarged diagram of  $u_{dc}$  in Fig. 6(f), the correctness of the proposed ZSVM6 algorithm is verified.

#### 4.2. Simulation results of AC side

The simulation waveforms of the AC side parameters of the ES-qZSI are shown in Fig. 7.

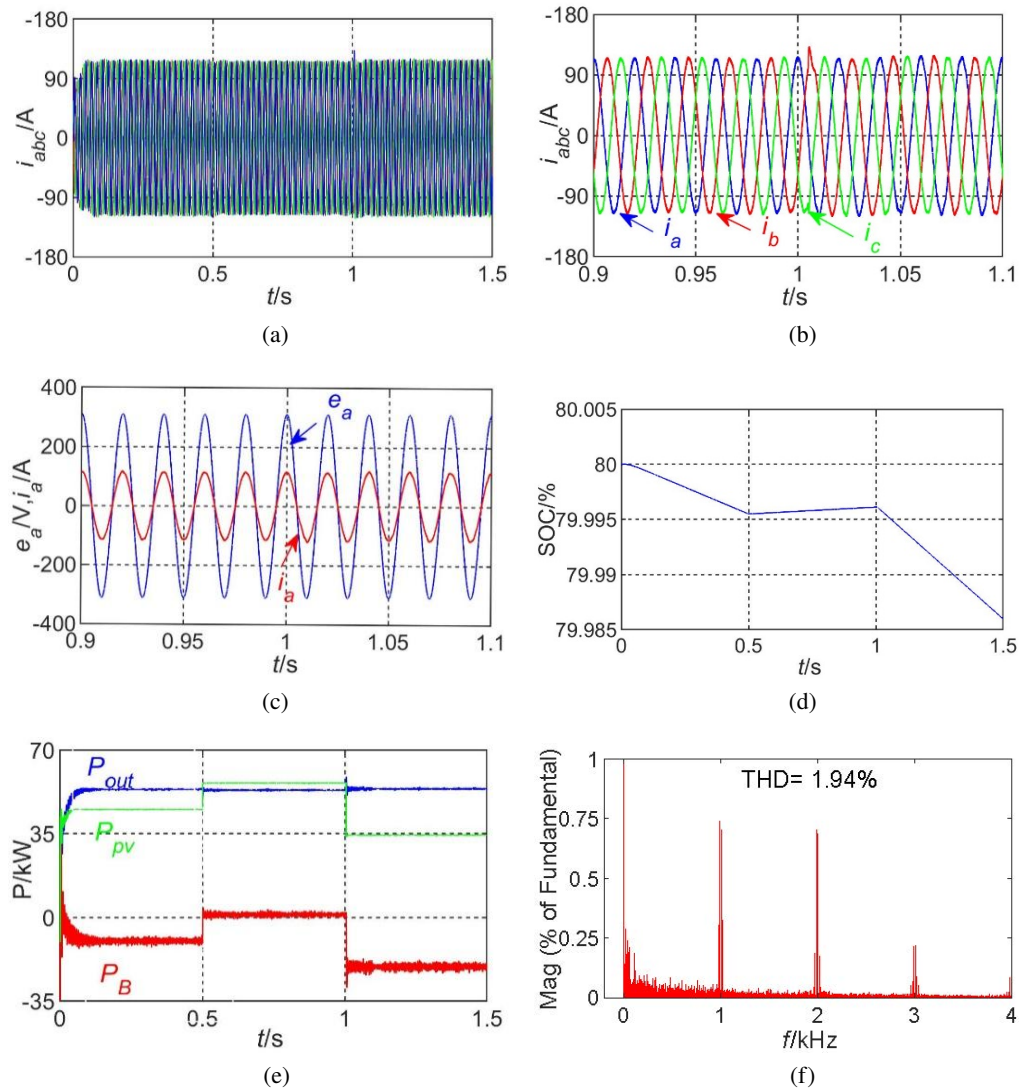


Fig. 7. Simulation results for AC side of ES-qZSI: three phase current waveform of grid-connected (a); three phase current waveform of grid-connected (0.9 ~ 1.1 s) (b); voltage and current waveform of A-phase (0.9 ~ 1.1 s) (c); SOC waveform of battery (d); power waveform of three phase(e); A-phase current spectrum analysis result (f)

Figure 7(a) and Fig. 7(b) are the grid-connected current waveforms and their partial diagrams. It can be seen that the grid-connected current fluctuates 0.02 s and then quickly returns to a stable state, which has good fast dynamic response performance and good current waveform quality. Figure 7(c) is the partial diagram of the voltage and current waveforms of the A-phase on the grid side. It can be seen that the frequency and phase of the A-phase voltage and current are the same, that is, there is no reactive power injected into the grid. Figure 7(d) and Fig. 7(e) is, respectively, the state of charge and three-terminal power waveform of the ES-qZSI battery. It can be seen that in 0 s ~ 0.5 s, the photovoltaic power is less than the grid-connected power, the SOC of the battery decreases, and the battery is in the discharge state, releasing its stored energy to compensate for the grid-connected power shortage. Within 0.5 s ~ 1 s, the photovoltaic power is greater than the grid-connected power, and the SOC of the battery increases, and the battery is in the charging state. The fluctuation of the grid-connected power is suppressed by absorbing excess power. Within 1 s ~ 1.5 s, the SOC of the battery decreases, and the battery discharges again. Figure 7(f) is the spectrum analysis diagram of the A-phase current in the network side of the system. Due to ZSVM6 control is added to MP-DPC method in the ES-qZSI system, the harmonics of the A-phase current in the grid side are mainly concentrated in the vicinity of the sampling frequency and its integral multiples, which solves the problem of large switching losses caused by unfixed switching frequency. The THD content of the A-phase current in the network side of the system is 1.94%, and the quality of the grid-connected current is high, which meets the requirements of the IEEE photovoltaic grid connection index.

## 5. Conclusions

Based on the traditional MP-DPC strategy, we proposed an improved MP-DPC strategy suitable for energy storage quasi-Z-source grid-connected inverters by combining SVPWM technology to fix the system switching frequency control. By analyzing the simulation results, the following conclusions were obtained.

1. The proposed control strategy not only realizes the control of photovoltaic input power, but also realizes the optimal control of active power and reactive power on the AC side of the inverter.
2. The PI controller and hysteresis controller in the traditional DPC strategy are replaced by the model predictive controller, which effectively reduced the current harmonics of the system and greatly improved the response speed and control accuracy.
3. The fixed switching signal can be generated by using ZSVM6 modulation, which can effectively reduce the switching losses during system operation, and the system has good dynamic and steady performance.

This paper only studies the ideal performance of power grid voltage balance. Next, it is necessary to analyze the model to predict the impact of direct power control on the system in different states, such as low voltage ride through.

### Acknowledgements

This research was supported by the National Natural Science Foundation of China (Nos. 61663021, 61763025, 61861025), the Provincial Key Research and Development Program of Gansu (18YF1FA058) as well as the Provincial Science and Technology Support Plan Program of Gansu (1304GKCA023).

## References

- [1] Ding M., Wang W.S., Wang X.L., Song Y.T., Chen D.Z., Sun M., *A Review on the Effect of Large-scale PV Generation on Power Systems*, Proceedings of the CSEE, vol. 34, no. 1, pp. 1–14 (2014), DOI: [10.13334/j.0258-8013.pcsee.2014.01.001](https://doi.org/10.13334/j.0258-8013.pcsee.2014.01.001).
- [2] Li Y., Fang F., Xiao X.Y., Zhang R., Li J.Y., Qi W.B., *Grid-connected photovoltaic control strategy based on input-output linearization for quasi-Z-source inverter*, High Voltage Engineering, vol. 45, no. 7, pp. 2167–2176 (2019), DOI: [10.13336/j.10036520.hve.20190628010](https://doi.org/10.13336/j.10036520.hve.20190628010).
- [3] Du Q., Gao F.Y., Qiao Y., *Quasi-PR Control Strategy for Quasi-Z Source PV Grid-connected Inverter Based on Power Feed-forward*, High Voltage Engineering, vol. 43, no. 10, pp. 3322–3329 (2017), DOI: [10.13336/j.1003-6520.hve.20170828001](https://doi.org/10.13336/j.1003-6520.hve.20170828001).
- [4] Li Y., Peng F.Z., *Constant Capacitor Voltage Control Strategy for Z-Source/Quasi-Z-Source Inverter in Grid-Connected Photovoltaic Systems*, Transactions of China Electrotechnical Society, vol. 26, no. 5, pp. 62–69 (2011), DOI: [10.19595/j.cnki.1000-6753.tces.2011.05.010](https://doi.org/10.19595/j.cnki.1000-6753.tces.2011.05.010).
- [5] Zhang B.G., Hong D.Y., Wang T.P., Zhen Z., Wang D.H., *A novel two-phase interleaved parallel bi-directional DC/DC converter*, Archives of Electrical Engineering, vol. 70, no. 1, pp. 219–231 (2021), DOI: [10.24425/aee.2021.136063](https://doi.org/10.24425/aee.2021.136063).
- [6] Qiu P.C., Ge B.M., Bi D.Q., *Battery energy storage-based power stabilizing control for grid-connected photovoltaic power generation system*, Power System Protection and Control, vol. 39, no. 3, pp. 29–33 (2011), DOI: [10.19595/j.cnki.1000-6753.tces.2011.05.010](https://doi.org/10.19595/j.cnki.1000-6753.tces.2011.05.010).
- [7] Kroics K., Zakis J., Suzdalenko A., Husev O., Khandakji K., *Operation possibility of grid-connected Quasi-Z-source Inverter with energy storage and renewable energy generation in wide power range*, Proceedings of 2017 IEEE First Ukraine Conference on Electrical and Computer Engineering, Kiev, Ukraine, pp. 564–569 (2017), DOI: [10.1109/UKRCO N.2017.8100303](https://doi.org/10.1109/UKRCO N.2017.8100303).
- [8] Li J.L., Ma H.M., Hui D., *Present Development Condition and Trends of Energy Storage Technology in the Integration of Distributed Renewable Energy*, Transactions of China Electrotechnical Society, vol. 31, no. 14, pp. 1–10+20 (2016), DOI: [10.19595/j.cnki.1000-6753.tces.2016.14.001](https://doi.org/10.19595/j.cnki.1000-6753.tces.2016.14.001).
- [9] Liu C., Zhuo J.K., Zhao D.M., Li S.Q., Chen J.S., Wang J.X., Yao Q., *A Review on the Utilization of Energy Storage System for the Flexible and Safe Operation of Renewable Energy Microgrids*, Proceedings of the CSEE, vol. 40, no. 1, pp. 1–18+369 (2020), DOI: [10.13334/j.0258-8013.pcsee.190212](https://doi.org/10.13334/j.0258-8013.pcsee.190212).
- [10] Han X.J., Liang Y.B., Wang M.Y., Li B., *Dual-regulating feedback optimization control method of PV combined energy storage system based on KF-MPC*, Acta Energiae Solaris Sinica, vol. 42, no. 1, pp. 56–62 (2021), DOI: [10.19912/j.0254-0096.tynxb.2018-0856](https://doi.org/10.19912/j.0254-0096.tynxb.2018-0856).
- [11] Wang J.H., Li H.D., *A new direct power control strategy of three phase boost type PWM rectifiers*, Proceedings of the CSEE, no. 16, pp. 47–52 (2005), DOI: [10.3321/j.issn:0258-8013.2005.16.009](https://doi.org/10.3321/j.issn:0258-8013.2005.16.009).
- [12] Ma J.P., Song W.S., Feng X.Y., *Direct Power Control of Single-phase Three-level Rectifiers Without Phase Locked Loop*, Proceedings of the CSEE, vol. 35, no. 7, pp. 1723–1731 (2015), DOI: [10.13334/j.0258-8013.pcsee.2015.07.021](https://doi.org/10.13334/j.0258-8013.pcsee.2015.07.021).
- [13] Zakaria El Z.L., Hocine B., Khalil N., *Dual Virtual Flux-based Direct Power Control for rectifier under harmonically distorted voltage condition*, Archives of Electrical Engineering, vol. 69, no. 4, pp. 951–966 (2020), DOI: [10.24425/aee.2020.134641](https://doi.org/10.24425/aee.2020.134641).
- [14] Jiang Y.S., Yu Y., Zhao H.M., *Direct Power Control of Three Phase PWM Rectifier Using Model Predictive Control*, Electric Drive, vol. 45, no. 7, pp. 21–25 (2015), DOI: [10.19457/j.1001-2095.2015.07.005](https://doi.org/10.19457/j.1001-2095.2015.07.005).
- [15] Yang X.W., Jiang J.G., *Predictive Direct Power Control for Three-phase Voltage Source PWM Rectifiers*, Proceedings of the CSEE, vol. 31, no. 3, pp. 34–39 (2011), DOI: [10.13334/j.0258-8013.pcsee.2011.03.005](https://doi.org/10.13334/j.0258-8013.pcsee.2011.03.005).

- [16] Ye H.Z., Jiang Y., Huang S.D., Xiao L., Liao W., *Deadbeat Predictive Direct Power Control for Three-Phase Voltage Source PWM Rectifiers*, Transactions of China Electrotechnical Society, vol. 30, no. 4, pp. 121–128 (2015), DOI: [10.19595/j.cnki.1000-6753.tces.2015.04.015](https://doi.org/10.19595/j.cnki.1000-6753.tces.2015.04.015).
- [17] Luo D.R., Ji X.H., Huang S., Liao W., *Model Predictive Direct Power Control for Three-Phase Voltage Source PWM Rectifiers*, Power System Technology, vol. 38, no. 11, pp. 3109–3114 (2014), DOI: [10.13335/j.1000-3673.pst.2014.11.025](https://doi.org/10.13335/j.1000-3673.pst.2014.11.025).
- [18] Zhao F.P., Yang Y., Ruan Y., Zhao C.J., *Comparative Study for Direct Power Control and Direct Power Predictive Control in Three-Phase Grid-Connected Inverters*, Transactions of China Electrotechnical Society, vol. 27, no. 7, pp. 212–220 (2012), DOI: [10.19595/j.cnki.1000-6753.tces.2012.07.028](https://doi.org/10.19595/j.cnki.1000-6753.tces.2012.07.028).
- [19] Ma J.P., Song W.S., Feng X.Y., *A Model Predictive Direct Power Control of Single-phase Three-level PWM Rectifiers*, Proceedings of the CSEE, vol. 36, no. 4, pp. 1098–1105 (2016), DOI: [10.13334/j.0258-8013.pcsee.2016.04.024](https://doi.org/10.13334/j.0258-8013.pcsee.2016.04.024).
- [20] Kulikowski K., *Modified algorithms of direct power control of AC/DC converter co-operating with the grid*, Archives of Electrical Engineering, vol. 61, no. 3, pp. 373–388 (2012), DOI: [10.2478/v10171-012-0030-2](https://doi.org/10.2478/v10171-012-0030-2).
- [21] Bouafia A., Gaubert J.P., Krim F., *Predictive Direct Power Control of Three-Phase Pulse width Modulation (PWM) Rectifier Using Space-Vector Modulation (SVM)*, IEEE Transactions on Power Electronics, vol. 25, no. 1, pp. 228–236 (2010), DOI: [10.1109/TPEL.2009.2028731](https://doi.org/10.1109/TPEL.2009.2028731).
- [22] Fang F., Li Y., Xiao X.Y., Qi W.B., You Y.F., Ding L.Y., *A Finite Control Set-model Predictive Control for Energy-stored Quasi-Z-source Inverter*, Proceedings of the CSEE, vol. 39, no. 7, pp. 2133–2144 (2019), DOI: [10.13334/j.0258-8013.pcsee.181131](https://doi.org/10.13334/j.0258-8013.pcsee.181131).
- [23] Cheng J., Xiao X.Y., Ma J.P., Yang X.Y., You Y.F., Cao Z.H., *Finite Switching Sequence Model Predictive Direct Power Control of a Three-phase Energy-stored Quasi-Z-source Grid-connected Inverter*, Power System Technology, vol. 44, no. 5, pp. 1647–1655 (2020), DOI: [10.13335/j.1000-3673.pst.2019.2150](https://doi.org/10.13335/j.1000-3673.pst.2019.2150).
- [24] Liu Y., Ge B., Abu-Rub H., Peng F.Z., *Overview of space vector modulations for three-phase Z-source/quasi-Z-source inverters*, IEEE Transactions on Power Electronics, vol. 29, no. 4, pp. 2098–2108 (2014), DOI: [10.1109/TPEL.2013.2269539](https://doi.org/10.1109/TPEL.2013.2269539).
- [25] Sun D.S., Ge B.M., Bi D.Q., Peng F.Z., *Analysis and control of quasi-Z source inverter with battery for grid-connected PV system*, International Journal of Electrical Power and Energy Systems, vol. 46, pp. 234–240 (2013), DOI: [10.1016/j.ijepes.2012.10.008](https://doi.org/10.1016/j.ijepes.2012.10.008).
- [26] Dong S., Zhang Q.F., Cheng S.K., *Inductor current ripple comparison between ZSVM4 and ZSVM2 for Z-source inverters*, IEEE Transactions on Power Electronics, vol. 31, no. 11, pp. 7592–7597 (2016), DOI: [10.1109/TPEL.2015.2475614](https://doi.org/10.1109/TPEL.2015.2475614).